Supporting Information

An Ultrastable Ti-based Metallocalixarene Nanocage Cluster with Photocatalytic Amines Oxidation Activity

Yi-Qi Tian[a]+, Yun-Shu Cui[b]+, Wei-Dong Yu[c], Cong-Qiao Xu*[b], Xiao-Yi Yi[a], Jun Yan[a], Jun Li,[b] Chao Liu*[a]

[a] College of Chemistry and Chemical Engineering, Central South University, Changsha 410083, Hunan, P. R. China

[b] Department of Chemistry, Southern University of Science and Technology, Shenzhen 518055, P. R. China.

[c] China College of Science, Hunan University of Technology and Business, Changsha 410000, P. R. China

Abstract: Polyhedral metallocalixarene nanocage clusters based on pure Ti(IV) ion are to our knowledge un-known hitherto. Herein we reported the first Ti(IV)-based metallocalixarene nanocluster by assembling a $[Ti_{13}O_{14}]$ cage with six t-butylcalix[4]arene molecules. Notably, the cluster exhibits extraordinary stability in high-concentration acid/alkali solutions and can act as a stable photocatalyst to catalyze the oxidation of ammonia to imines.

1. experimental section

Materials and Characterization. All reagents were purchased commercially and were not further purified when used. Powder X-ray diffraction (PXRD) analysis were performed on a Rigaku Mini Flex II diffractometer at a 2θ range of 3–50° (5° min^{-1}) with CuK_α radiation (λ =1.54056 Å). The solid-state UV/Vis spectrum of the cluster was obtained on UV-4000 spectrophotometer. Mass spectra was recorded on an Autoflex Speed MALDI-TOF MS (Bruker) spectrometer. Thermogravimetric (TGA) pattern was recorded on a Mettler Toledo TGA/SDTA 851e analyzer in a N_2 atmosphere. FT-IR spectra using KBr pellets were taken on a Bruker Vertex 70 Spectrometer. Dynamic light scattering (DLS) measurement is performed on a Malvern Zetasizer 1000HSA.

X-ray Crystal Structure Determination. Single crystal diffraction data in the paper were collected on Rigaku XtalAB Synergy DS diffractometer with graphite monochromated Cu Kα radiation. The structures were solved using intrinsic phasing methods in ShelXT program and then refined by full-matrix least-squares on F^2 using ShelXL-2014 in Olex^2 program. The hydrogen atoms were introduced at their geometric positions and refined as riding atom, and the positions of non-hydrogen atoms were refined with anisotropic displacement parameters during the final cycles. Due to the rotation disorder of tert-butyl groups, in all cases the ISOR, DELU and SIMU constraints were necessary to achieve convergence. The SQUEEZE operation was used to eliminate the contribution of disordered solvent molecule to the reflection intensity. Rotational disorder of the cluster was found in the **{$Ti_{13}L_6$}**, and this was modeled accordingly (see the Figure S1). A summary of the crystallographic data for the reported clusters is listed in Table S1. CCDC **2101667** contain the crystallographic data herein.

Synthesis for {$Ti_{13}(\mu_3\text{-}O)_8(\mu_4\text{-}O)_6(TBC[4])_6$}·$6CH_3CN$ ({$Ti_{13}L_6$}): TBC[4] (42 mg, 0.065 mmol) and 4'-(pyridin-4-yl)-[1,1'-biphenyl]-3,5-dicarboxylic acid (32 mg, 0.1 mmol) were sealed in a 25mL Teflon-lined reaction vesse with 5 mL CH_3CN. $Ti(O^iPr)_4$ (100 μL, 0.33 mmol) was added dropwise. The resulting mixtures were then transferred to a preheated oven at 100 °C for 4 days. After cooling to 25°C, red crystals were obtained with a low yield of about 10%, accompanied by a large amount of white precipitates. Elem. Anal. Calcd for $C_{276}H_{330}O_{38}N_6Ti_{13}$ (wt%): C,66.68; H, 6.23; O, 12.05. Found: C, 64.77; H, 7.219; O, 13.57. The elemental analysis results are somewhat different from the theoretical values, which may be caused by impurities on the crystal surface.

Photocurrent responses. Photoelectrochemical tests were carried out on a CHI 660E electrochemical workstation. The platinum plate was used as the counter electrode, and the saturated calomel electrode was used as the reference electrode. 5 mg crystal samples were ultrasonically dispersed in 1 ml ethanol, and then the dispersion was dropped on FTO glass to prepare the working electrode. The electrodes were immersed in the 0.2 M Na_2SO_4 aqueous solution. A 300 W Xe lamp with UV cut-off filter was used as a full-wavelength light source.

Contact Angle Measurements. Contact angles were measured on powder samples using a contact angle meter with a rotatable substrate holder. To perform contact angle measurements, 20 mg of powder samples of the clusters were deposited on a glass substrate bed. Then, powders were pressed to make a flat surface by the glass slide. A 10 μL water droplet was released slowly on the flat surface of the powder samples. The droplet image was taken by a high-performance charge-coupled device (CCD) sensor. The contact angle of all powder samples was analyzed by five-point simulation analysis.

Typical procedure for the oxidation of amines. The photocatalytic reactions were carried out under irradiation by a Xe lamp (300 W, PLS-SXE 300, Beijing Trusttech Co.) equipped with a cutoff filter to filter out light below 420 nm and a broad band filter to cutoff light above 750 nm, with magnetic stirring in a 10 mL Pyrex glass bottle. The bottle was sealed with a rubber stopper wrapped in aluminum foil. Benzylamine (1 mmol), catalyst (0.02 mmol), H_2O_2 (100 μL) and solvent (2 mL) were added in a glass bottle. The reaction was stirred at 60°C under Xe lamp. After reaction, the mixtures were analyzed by GC and ^{1}H NMR. The catalysts were collected by filtration and washed with CH_3CN, and reused for the next catalytic reaction.

Computational Method Quantum chemistry calculations were performed using density functional theory (DFT) implemented in Gaussian16 program[1] with PBE functional.[2] The def2-SVP basis set[3] was utilized for Ti atom and STO-3G for other elements in geometry optimizations, while def2-TZVP basis sets[3] were used for Ti and def2-SVP for other elements in single point calculations. SMD solvation model[4] was applied in calculating hydration energy of **{$Ti_{13}L_6$}·H_2O**. The solvation free energy was calculated as follows: $\Delta G_{(solv)}=E_{(SMD,\ water)}-E_{(gas)}$,[4,5] where $E_{(SMD,\ water)}$ and $E_{(gas)}$ refer to the electronic energy in the presence and absence of the SMD solvent field which were calculated with M05-2X[6] functional and 6-31g* basis set.

References:

1. Frisch, M. J.; Trucks, G. W.; Schlegel, H. B.; Scuseria, G. E.; Robb, M. A.; Cheeseman, J. R.; Scalmani, G.; Barone, V.; Petersson, G. A.; Nakatsuji, H., Gaussian, Inc. Wallingford, CT. 2016.

2. Perdew, J. P.; Burke, K.; Ernzerhof, M. Generalized gradient approximation made simple. *Phys. Rev. Lett*. 1996, 77, 3865-3868.

3. Weigend, F.; Ahlrichs, R. Balanced basis sets of split valence, triple zeta valence and quadruple zeta valence quality for H to Rn: Design and assessment of accuracy. *Phys. Chem. Chem. Phys*., **2005**, *7*, 3297-3305.

4. Marenich, A. V.; Cramer, C. J.; Truhlar, D. G. Universal solvation model based on solute electron density and a continuum model of the solvent defined by the bulk dielectric constant and atomic surface tensions. *J. Phys. Chem. B*, **2009**, *113*, 6378-6396.

5. Ho, J.; Klamt, A.; Coote, M. L. Comment on the Correct Use of Continuum Solvent Models. *J. Phys. Chem. A* **2010**, *114* (51), 13442−13444.

6. Zhao, Y.; Schultz, N. E.; Truhlar, D. G. Design of Density Functionals by Combining the Method of Constraint Satisfaction with Parametrization for Thermochemistry, Thermochemical Kinetics, and Noncovalent Interactions, *J. Chem. Theory Comput.*, **2006**, *2*, 364.

2. Structure of {$Ti_{13}L_6$} Compound

Compounds	**{$Ti_{13}L_6$}**
CCDC	**2101667**
Formula	$C_{276}H_{330}O_{38}N_6Ti_{13}$
T(K)	150.0
F_w	4715.82
Crystal system	tetragonal
Space group	I4/m
a, Å	23.2672(11)
b, Å	23.2672(11)
c, Å	25.827(2)
V/Å^3	13981.7(17)
Z	2
ρ_{calcd}/gcm^{-3})	1.120
μ/mm^{-1})	2.223
F(000)	4972
Data/restraints/parameters	6664/174/501
Goof	1.082
R_1/wR_2(I> 2σ(I))	0.1035/0.2084

R_1/wR_2(all data)	0.1096/0.2104

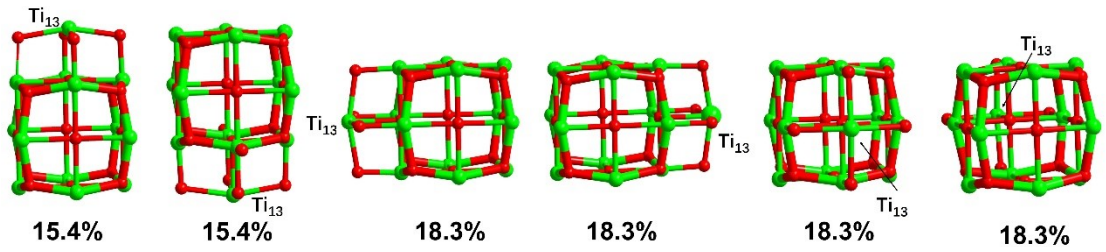

Figure S1. Disordered structure model of $Ti_{13}O_{14}$ cage in **{$Ti_{13}L_6$}** cluster. The Ti13 ion is distributed on the six faces of the $Ti_{12}O_{14}$ cubic cage, and the total occupation ratio is 1.

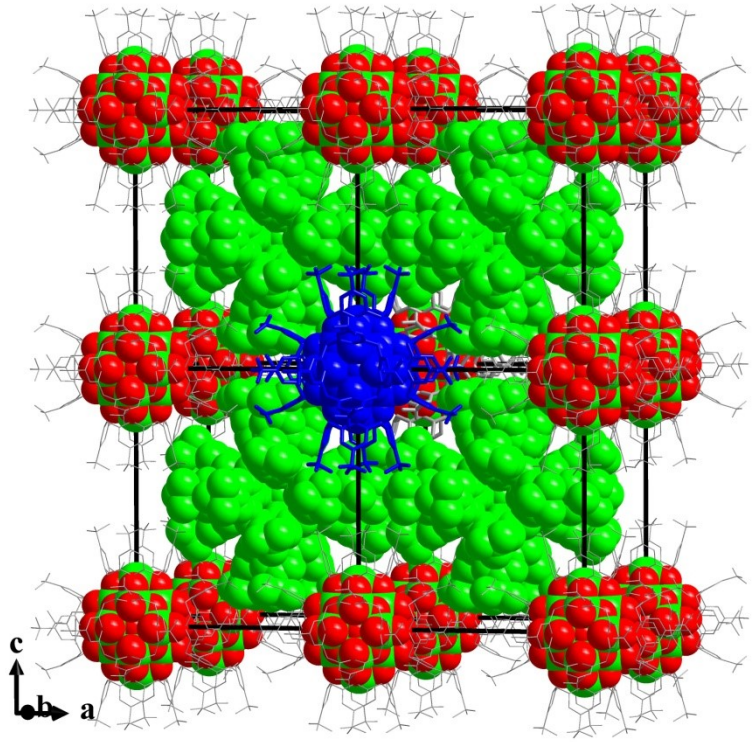

Figure S2. Body-centered cubic packing of the **{$Ti_{13}L_6$}.**

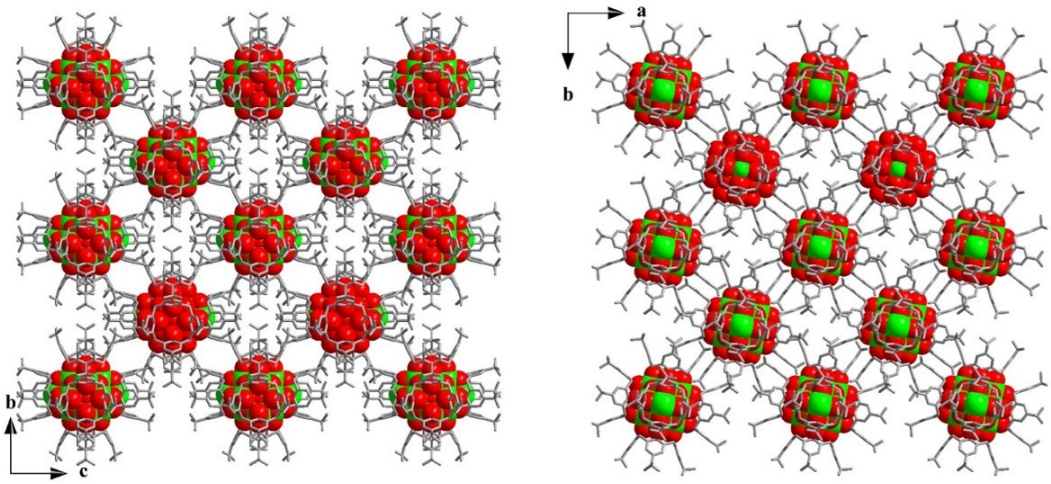

Figure S3. Three-dimensional packing structure of **{$Ti_{13}L_6$}** along the *a* axis (A) and *c* axis (B).

3. Energy Dispersive X-ray (EDX) Spectroscopic Analysis

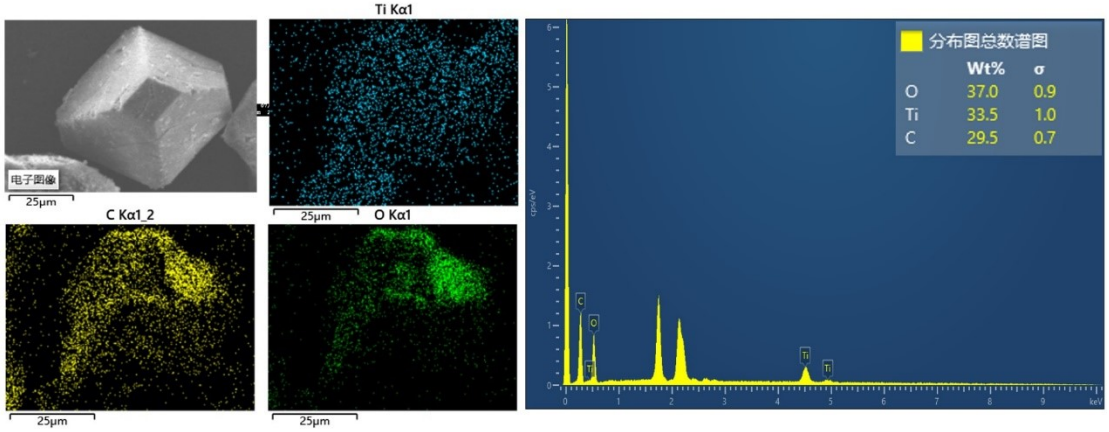

Figure S4. The SEM and EDS pattern of **{$Ti_{13}L_6$}**.

4. XPS Measurement

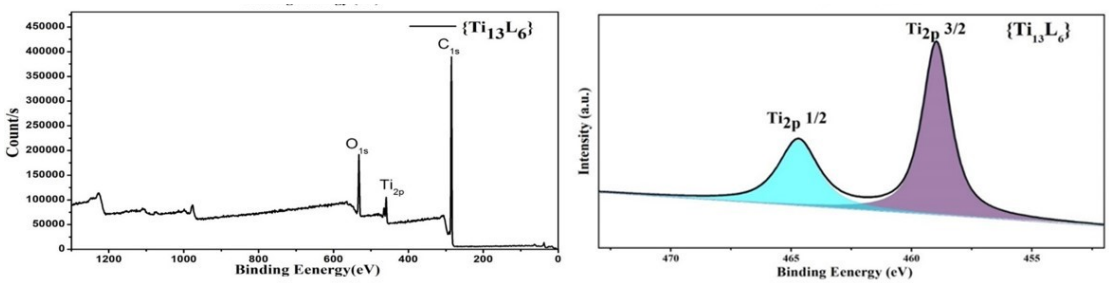

The existence of Ti^{4+} has been confirmed by the XPS test. The Ti 2p spectrum clearly shows two regions of Ti $2p^{1/2}$ (ca. 464.9 eV) and Ti $2p^{3/2}$ (ca. 459.0 eV) with 5.9 eV binding energy difference, being indicative of the unique existence of Ti^{4+}.

Figure S5. XPS Measurement for **{$Ti_{13}L_6$}**.

5. Dynamic light scattering experiment

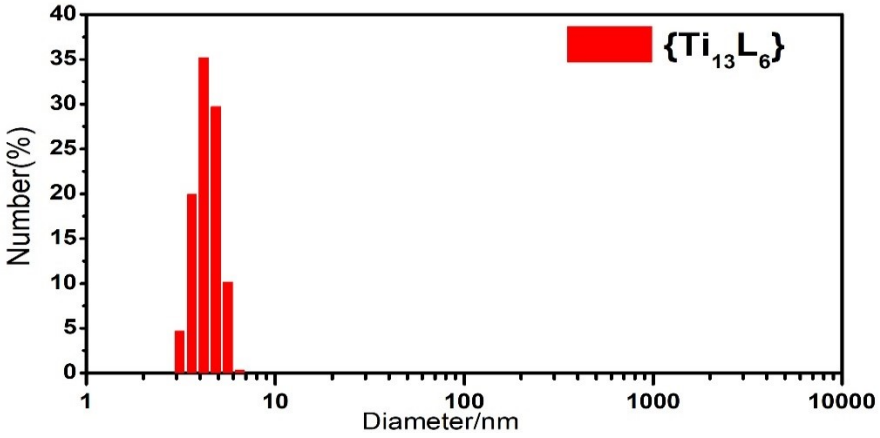

Figure S6. Size distribution obtained from the **{$Ti_{13}L_6$}** nanocage-dichloromethane solution.

6. Powder X-ray diffraction

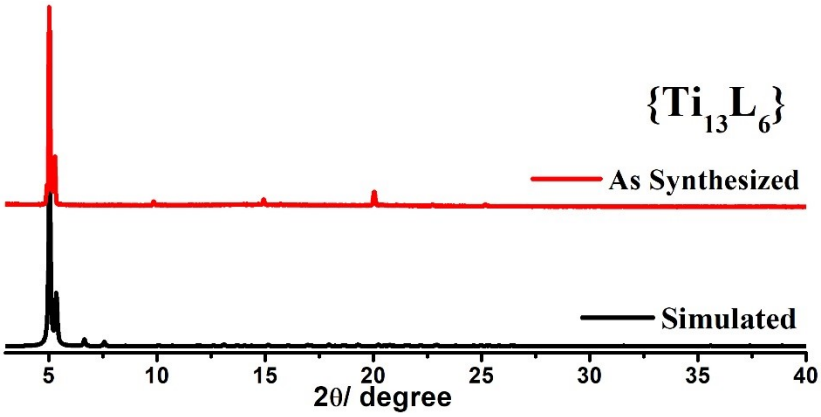

Figure S7. The XRD pattern of **{$Ti_{13}L_6$}**.

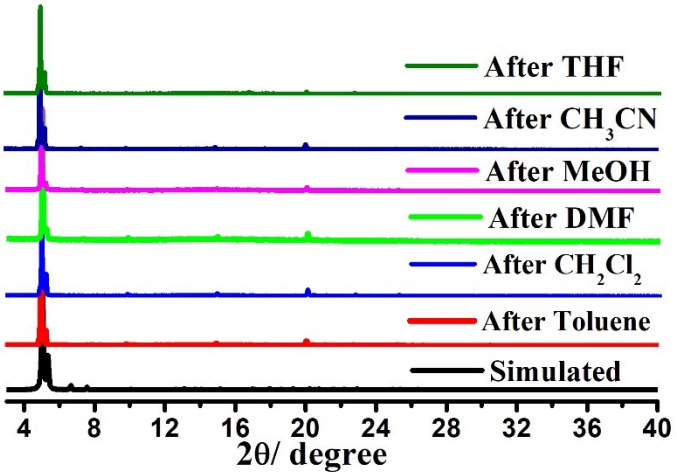

Figure S8. PXRD patterns of **{$Ti_{13}L_6$}** after being treated in different organic solvents for 24 h.

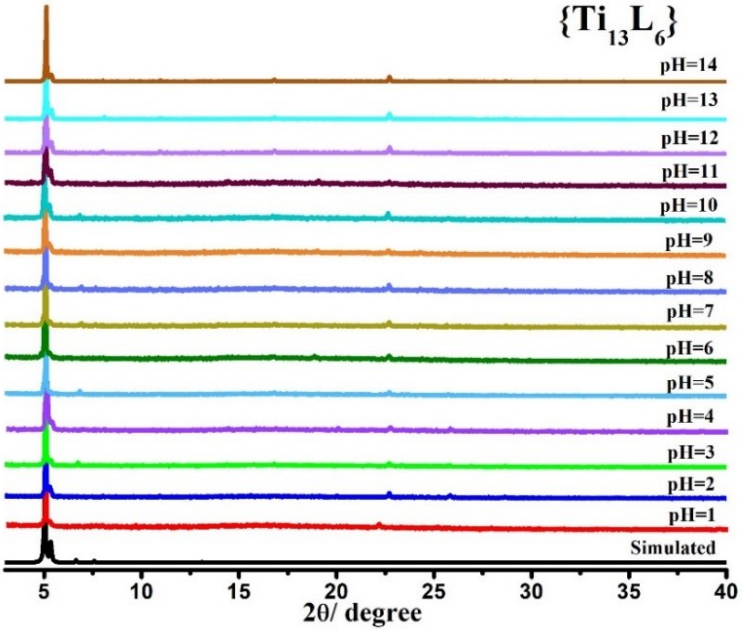

Figure S9. The XRD pattern of **{$Ti_{13}L_6$}** treated in different pH solutions.

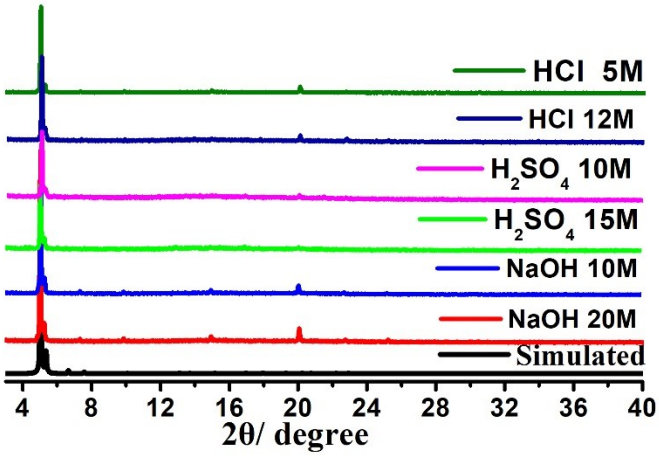

Figure S10. PXRD patterns of {$Ti_{13}L_6$} after being treated in high concentrated acid/alkali solution for 24 h.

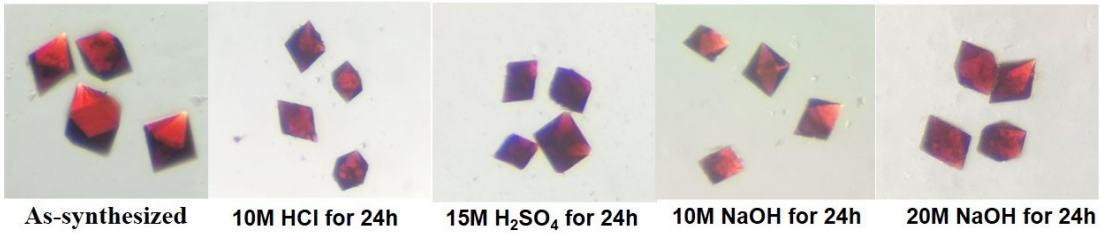

Figure S11. Photographs of fresh crystals and crystal samples after soaking in 15M H_2SO_4, 12M HCl, 10 M NaOH and 20 M NaOH solutions for 24 hours.

Table S2: Crystallographic data of $Ti_{13}L_6$ after treatment in basic media of 20M NaOH.

Conditions	as-synthesized	**Soak in 20M NaOH solution for 72h**
t [h]	0	72
Cryst. syst.	tetragonal	tetragonal
Space group	I4/m	I4/m
A[Å]	23.2672(11)	23.3694(9)
b[Å]	23.2672(11)	23.3694(9)
c[Å]	25.827(2)	25.555(4)
V[Å^3]	13981.7(17)	13956(2)
Goof	1.082	1.106
R1/wR_2(I> 2σ(I))	0.1035/0.2084	0.1330/0.4167
R1/wR_2(all data)	0.1096/0.2104	0.1796/0.4742

7. IR spectrum

Figure S9 shows the FTIR spectra of cluster. The broad band between 3200-3500 cm^{-1} attributable to OH stretching. The strong vibration band at ca. 1620-1650 cm^{-1} can be ascribed to C=O stretching of the carboxyl. The characteristic bands of Ti-O-C and Ti-O-Ti appears in the ranges of 1000–1200 and 700–800 cm^{-1}, respectively.

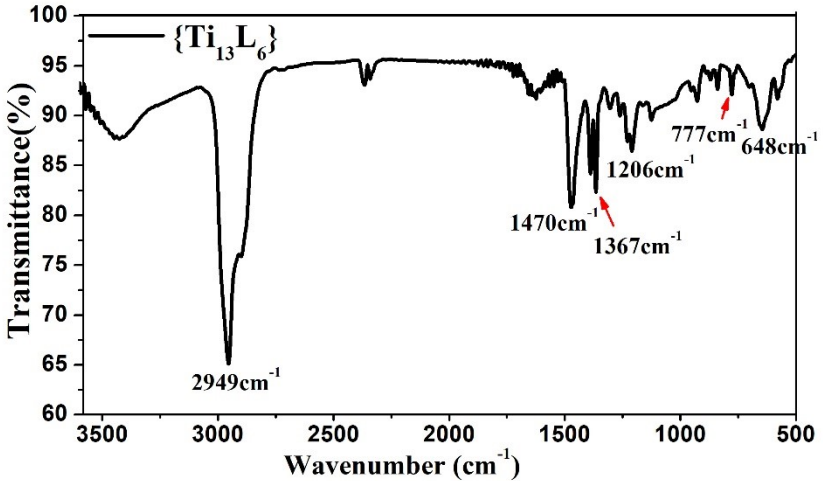

Figure S12. IR spectrum of crystal sample of $\{Ti_{13}L_6\}$.

8. TG-Measurement

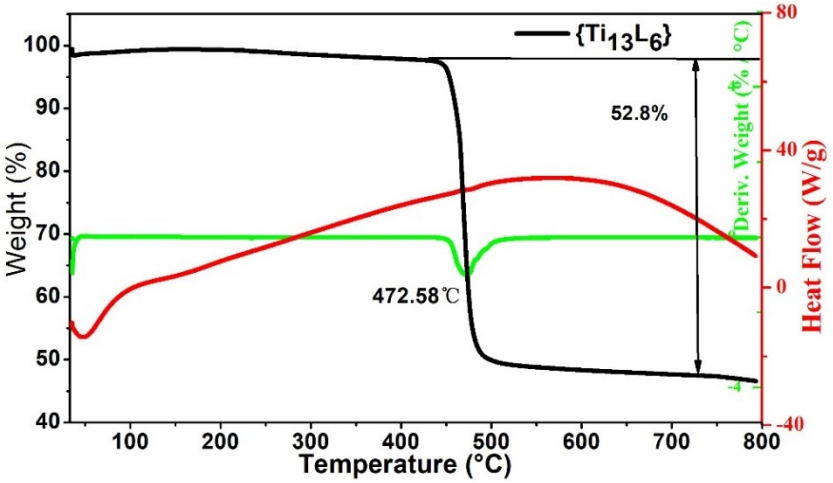

Figure S13. The TGA and DSC curves of $\{Ti_{13}L_6\}$.

9. Theoretical calculation

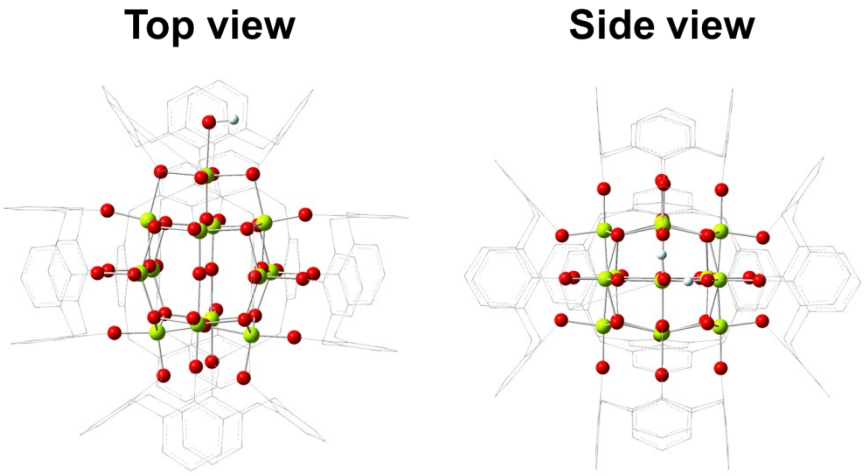

Figure S14. Top view and side view of $\{Ti_{13}L_6\}\cdot H_2O$. The tert-butyl groups of TBC[4] are omitted for clarity.

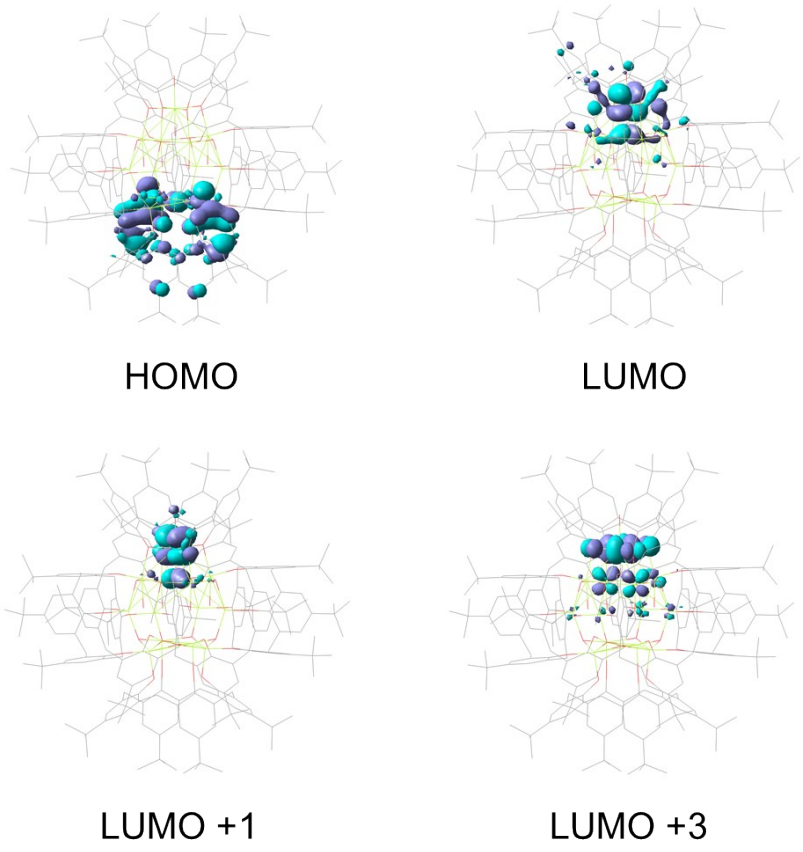

Figure S15. Contour plots of HOMO, LUMO, LUMO+1 and LUMO+3 (Isovalue = 0.03 a.u.).

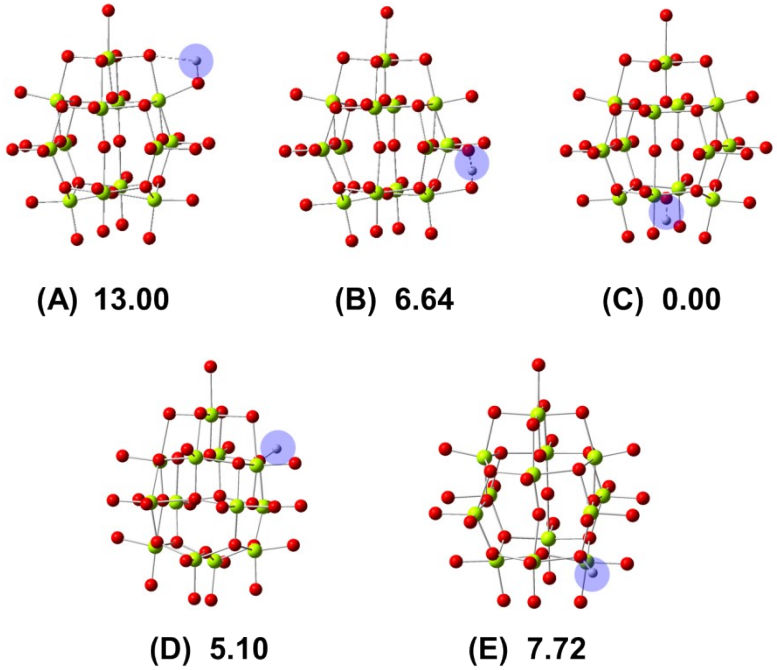

Figure S16. Optimized structures and relative energy values (in kcal/mol) for five isomers of $\{Ti_{13}L_6H\}^{+\cdot}H_2O$. Carbon and hydrogen (except the coordinated proton) atoms are omitted for clarity.

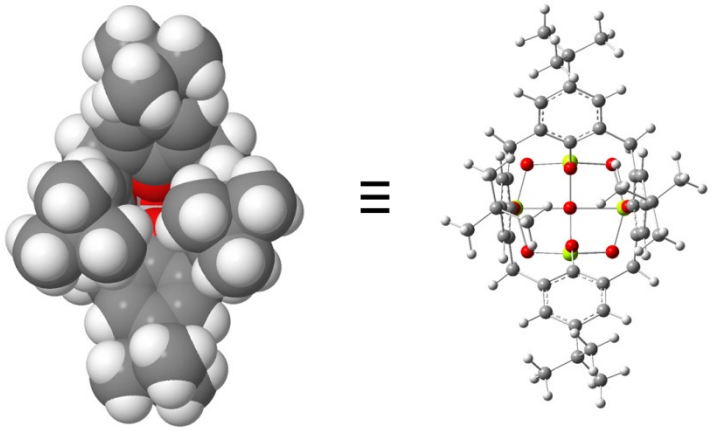

Figure S17. Space-filling model of the cavity surrounded by a TBC[4] ligand that corresponds to the most favorable protonation site in **{$Ti_{13}L_6$}·H_2O** (isomer C in Figure c). Other atoms are omitted for clarity.

Table S3. Average bond length values (in Å) in optimized structures for **{$Ti_{13}L_6$}·H_2O** and five isomers of **{$Ti_{13}L_6H$}$^+$·H_2O**. [a]

	{$Ti_{13}L_6$}·H_2O[b]	Isomers of **{$Ti_{13}L_6H$}$^+$·H_2O**				
		(A)	(B)	(C)	(D)	(E)
Ti(13)-O(a)	1.91(2.14)	1.91	1.91	1.91	1.91	1.91
Ti(13)-O(c)	1.79(2.17)	1.81	1.79	1.79	1.79	1.80
Ti(a)-O(a)	2.11(1.83)	2.13	2.08	2.09	2.11	2.09
Ti(a)-O(b)	1.76(1.83)	1.78	1.75	1.75	1.76	1.76
Ti(a)-O(c)	2.19(2.18)	2.21	2.21	2.25	2.23	2.21
Ti(a)-O(d)	1.94(1.92)	1.95	1.94	1.93	1.97	1.96

[a] O(a): Oxygen atoms in the TBC[4] ligand that coordinate to Ti13. O(b): Other oxygen atoms in the TBC[4] ligands. O(c): Oxygen atoms in the face centers of the $Ti_{12}O_{14}$ cube. O(d): Oxygen atoms at the vertices of the $Ti_{12}O_{14}$ cube. Ti(a): Titanium atoms in the $Ti_{12}O_{14}$ cube.

[b] Bond length values in parentheses are obtained from the crystalline structure in experiment.

Table S4. Energy values of $\Delta G_{(solv)}$, $E_{(SMD,\ water)}$ and $E_{(gas)}$ of **{$Ti_{13}L_6$}·H_2O** in Hartree/particle.

Energy term	
$E_{(SMD,\ water)}$	0.0670037 [a]
$E_{(gas)}$	-24227.0356385
$\Delta G_{(solv)}$	-24226.9686348

[a] This value is 42.05 in kcal/mol.

10. Contact angle test

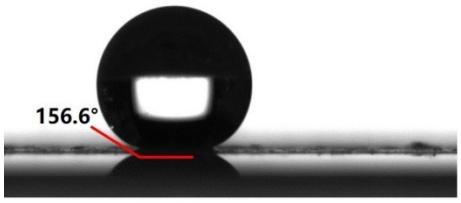

Figure S18. Contact angle pattern for **{$Ti_{13}L_6$}**.

11. Solid state UV-Vis spectrum

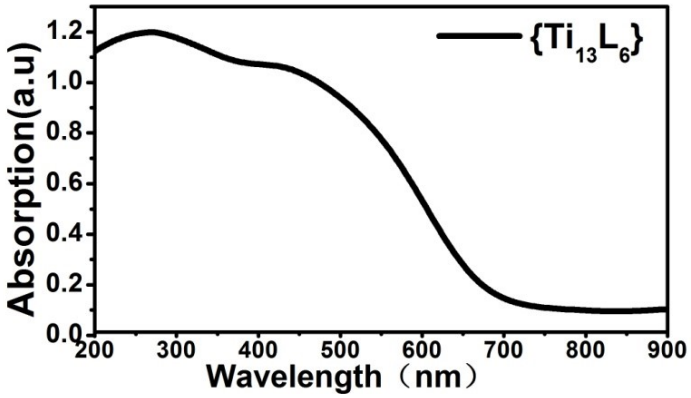

Figure S19. Solid state UV-Vis spectrum of the $\{Ti_{13}L_6\}$ cluster.

12. Photocurrent response

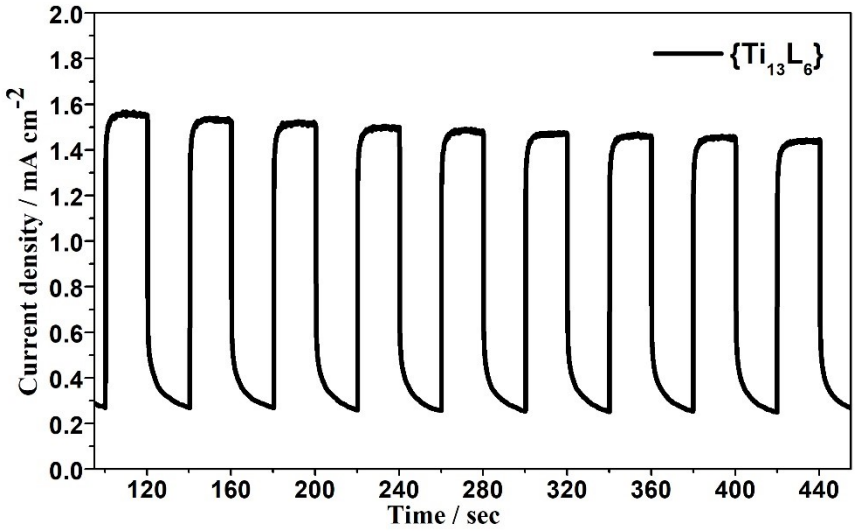

Figure S20. Photocurrent responses of the **$\{Ti_{13}L_6\}$** in 0.2 M Na_2SO_4 (pH= 6.8) aqueous solution under repetitive irradiation (λ > 420 nm; 300 W; intervals of 20 s)

13. Photocatalysis

Table S5. The optimization of different reaction conditions of benzylamine to *N*-benzylidine-1-phenylmethanamine [a]

Entry	Cat.	Oxidant	Time	Addition	Yield [b]
1	**$\{Ti_{13}L_6\}$**	H_2O_2(30% 100 μL)	2	/	20.8%
2	**$\{Ti_{13}L_6\}$**	H_2O_2	4	/	37.5%
3	**$\{Ti_{13}L_6\}$**	H_2O_2	6	/	62.3%
4	**$\{Ti_{13}L_6\}$**	H_2O_2	8	/	79.0%
5	**$\{Ti_{13}L_6\}$**	H_2O_2	10	/	90.6%
6	**$\{Ti_{13}L_6\}$**	H_2O_2	12	/	99.9%
7	**$\{Ti_{13}L_6\}$** (Second cycle)	H_2O_2	12	/	99.5%
8	**$\{Ti_{13}L_6\}$** (Third cycle)	H_2O_2	12	/	98.9%
9	**$\{Ti_{13}L_6\}$** (Fourth cycle)	H_2O_2	12	/	98.3%
10	**$\{Ti_{13}L_6\}$** (Fifth cycle)	H_2O_2	12	/	97.8%
11	**$\{Ti_{13}L_6\}$** (No light)	H_2O_2	2	/	10.6%

12	**{$Ti_{13}L_6$}** (No light)	H_2O_2	4	/	20.7%
13	**{$Ti_{13}L_6$}** (No light)	H_2O_2	6	/	25.4%
14	**{$Ti_{13}L_6$}** (No light)	H_2O_2	8	/	28.5%
15	**{$Ti_{13}L_6$}** (No light)	H_2O_2	10	/	31.0%
16	**{$Ti_{13}L_6$}** (No light)	H_2O_2	12	/	34.6%
17	**{$Ti_{13}L_6$}**	O_2	12	/	22.0%
18	/	H_2O_2	12	/	1.1%
19	**TiO_2+TBC[4]**	H_2O_2	12	/	8.1%
20	**TiO_2+TBC[4]** (No light)	H_2O_2	12	/	4.1%
21	**TiO_2**	H_2O_2	12	/	8.3%
22	**TBC[4]**	H_2O_2	12	/	2.6%
23	/	H_2O_2	12	/	1.1%
24	**{$Ti_{13}L_6$}**	/	6	/	4.8%
25	**{$Ti_{13}L_6$}**	H_2O_2	12	benzoquinone	18.7%
26	**{$Ti_{13}L_6$}**	H_2O_2	12	EDTA-2Na	2.7%
27	**{$Ti_{13}L_6$}**	H_2O_2	12	$Mn(CH_3COO)_2$	6.5%

[a] Reaction conditions: substrate, benzylamine (110 μL, 1 mmol), catalyst (0.02 mmol), H_2O_2 (100 μL), solvent (2 mL), Xe lamp. [b] Determined by GC analysis and ^{1}H NMR.

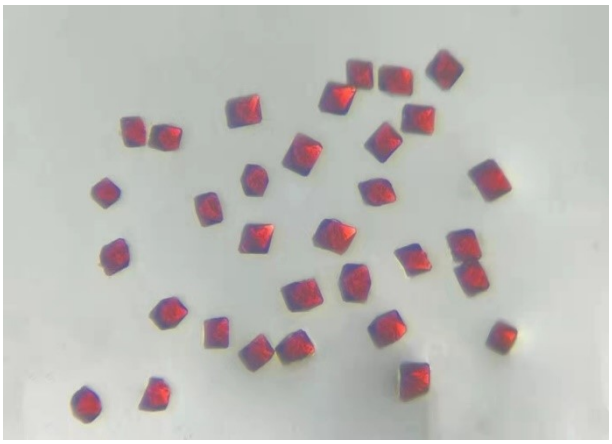

Figure S21. The crystal photos of **{$Ti_{13}L_6$}** after one cycle photocatalysis test. The high quality of retrieved single crystals confirmed the stability of **{$Ti_{13}L_6$}** during the photocatalysis tests.

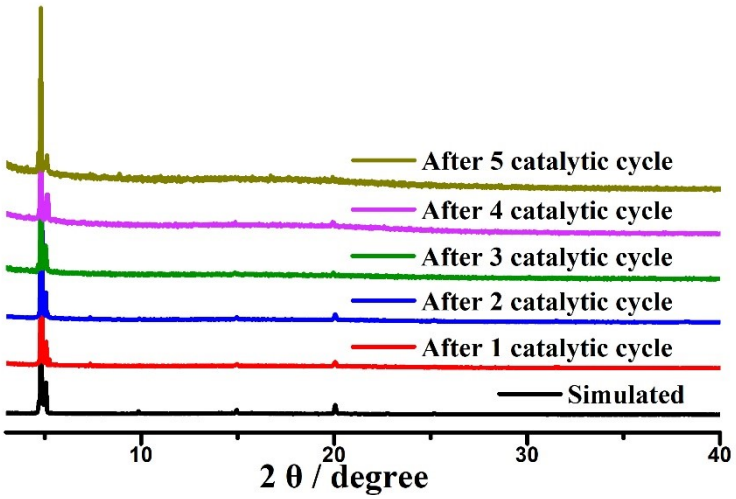

Figure S22. PXRD patterns of **{$Ti_{13}L_6$}** after catalytic tests.

Table S6: Crystallographic data of **{$Ti_{13}L_6$}** after photocatalytic reaction (after one cycle).

Conditions	as-synthesized	After photocatalytic reaction
Cryst. syst.	tetragonal	tetragonal
Space group	I4/m	I4/m
A[Å]	23.2672(11)	23.228(4)
b[Å]	23.2672(11)	23.228(4)
c[Å]	25.827(2)	26.018(6)
V[Å^3]	13981.7(17)	13956(2)
Goof	1.082	1.106
R1/wR_2(I> 2σ(I))	0.1035/0.2084	0.0841/0.2547
R1/wR_2(all data)	0.1096/0.2104	0.0923/0.2644

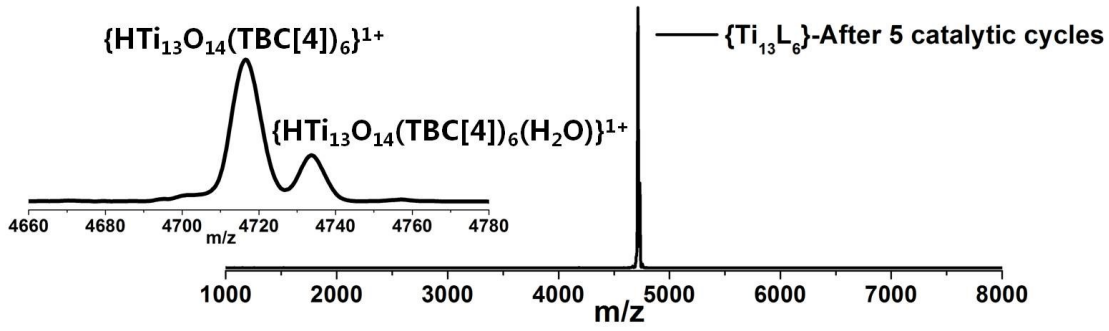

Figure S23. Positive-mode MALDI-TOF-MS spectrum of the crystalline sample of **{$Ti_{13}L_6$}** after five catalytic cycles.

Table S7. The ICP result of filtrate after five catalytic cycles.

Filter liquor	The leakage of Ti^{4+}
After five cycles	0.0245%